2019-11-14

Testing and Characterization of Different Papers as Substrate Material for Printed Electronics and Application in Humidity Sensor

Tijana Kojić, Goran Stojanović, Aleksandar Miletić, Milan Radovanović, Hani Al-Salami, Fabiana Arduini

Sensors and Materials, Vol. 3#, No. # (201#) ##–##
MYU Tokyo

S & M ****

Testing and Characterization of Different Papers as Substrate Material for Printed Electronics and Application in Humidity Sensor

Tijana Kojić,[1] Goran M. Stojanović,[1*] Aleksandar Miletić,[1] Milan Radovanović,[1] Hani Al-Salami,[2] and Fabiana Arduini[3]

[1]University of Novi Sad, Faculty of Technical Sciences, Trg Dositeja Obradovića 6, 21000 Novi Sad, Serbia
[2]Curtin Health Innovation Research Institute, Curtin University, 6102 Perth WA, Australia
[3]Department of Chemical Science and Technologies, University of Rome "Tor Vergata", 00133 Rome, Italy

(Received Month Day, Year; accepted Month Day, Year; online published Month Day, Year)

Keywords: paper, printed and flexible electronics, characterization, humidity sensor

The use of papers as substrates in the process of manufacturing flexible electronic components is urgently required to obtain cost-effective products as well as to expand the potential applications. This study aimed to examine the suitability of three different types of paper for sensor applications using an inkjet printing process. Three types of paper (denoted with *Type 1*, *Type 2*, and *Type 3*) designed for specific applications in the printed electronics were selected and entirely characterized in terms of microscopic and macroscopic properties, such as, internal fibers structure, cross–sectional layers structure, surface roughness, and hardness. Dot arrays were printed on these three types of paper to determine how the papers absorb silver ink and which one is the best as a substrate for manufacturing printed electronic components. After a comprehensive analysis, the paper that exhibited the best feature was further studied as a substrate for printing interdigitated electrodes to develop a humidity sensor. The *Type 2* paper-based sensor demonstrated the variation of capacitance in the range from 9.4 pF to 10.6 pF while changing relative humidity from 40% to 90%. Thus, the paper *Type 2* has the great potential for application in flexible sensors, and suggesting possibility for the industrial scalability and mass production of inexpensive, biodegradable, and conformable electronic components.

1. Introduction

There is a need for electronic devices with superior performance, robustness, smaller size, cost–effectiveness, user friendliness, and lower environmental impact.(1) Printed electronics is a rapidly emerging and innovative technology for the fabrication of electronic devices. Printed/flexible electronics enables the fabrication of electronic components on mechanically flexible substrates, such as plastic, paper, and textiles, using electrically functional inks and low-cost fabrication processes.(2) The cost–effectiveness, flexibility, and bendability of these

*Corresponding author: e-mail: xxxxxxxx@xxx.edu.jp
https://doi.org/10.18494/SAM.2018.####

ISSN 0914-4935

substrates are attractive for high-performance foldable devices.[3] When dealing with flexible devices, the substrate plays an important role in hosting a variety of insulating, semiconducting, and conductive materials or components. Paper can be a good choice for a mechanically flexible substrate in printed electronics, because it is widely available and well-established in the printing and packing industries, it is biodegradable and lightweight, and it can be folded into different shapes and three–dimensional (3D) configurations. Furthermore, paper is a cost-effective and recyclable substrate compared with plastic substrates such as polyethylene terephthalate (PET) since it is made of renewable raw materials. By employing the advantages of paper substrates, electronic circuits and sensors printed on paper are sustainable and capable of remaining functional, when folded at various angles and after repeated folding. Paper–based circuits and sensors can be easily trimmed by a pair of scissors and folded into complex shapes.[4] Moreover, electronic components can be connected on both sides of a paper substrate, and paper substrates may be useful for applications in adhesive medical electrodes or low-cost portable diagnostic tools, exploiting the porosity of the paper.[5] Paper is presently available with various compositions, thicknesses, surface roughness, weights, strengths, prices, and wetting properties. Different types of paper have been used as substrates for flexible electronic components, circuits, and electrochemical sensors. These include (a) Teslin paper (PPG Industry, USA),[4] (b) pigment (kaolin)–coated paper (with a thickness of 130 μm and grammage of 126 g/m^2),[6] (c) glossy–finished photo paper (Epson C13S042187),[7] (d) coated paper with a density of 65 g/m^2, thickness of 76 μm, and dielectric constant near 1.2 (Ahltrom manufacturer's data),[8] (e) conventional printing paper from Gimba, SP, Brazil,[9] Fabriano Copy 2 (80 g/m^2) and Fabriano Multip@per office paper (100 g/m^2),[10] and filter paper (67 g/m^2, Cordenons, Italy).[11] In the manufacturing processes, dry fabrication techniques have been usually employed, such as screen printing, inkjet printing,[8] or a pen–on–paper approach.[12] Different types of paper can also be used for biosensor manufacturing, and various fabrication methods from wax printing to origami–inspired approaches can be applied.[13] Paper–electrode–based flexible pressure sensor modified with Multiwall Carbon Nanotubes (MWCNTs) was reported in Ref. (14). For applications in sensors, paper is a promising candidate owing to its porous structure and rough surface.[15] The mechanical characterization of paper sheets was reported in Refs. (16) and (17), and a very good sensitivity towards changes in moisture and temperature was shown.

In the manufacturing process of electronic components and sensors, the characteristics of the used paper impact the features of the final products. Although, the producers of different types of paper provide limited information in date sheets such as the surface free energy of the front and reverse sides, weight, whiteness, temperature resistance, and printability, these data are not enough for researchers and professionals for electronic component development. The objectives of this study is to provide detailed information about internal and surface characteristics of analyzed papers and to connect them with the performances of the paper as a substrate for inkjet printed sensor applications.

Herein, we give a complete characterization of three types of paper intended to be used as substrates in printed or flexible electronics. Three commercially available papers from Felix Schoeller Group[18] were selected from the specific series p_e:smart® which are denoted as *Type 1*, *Type 2*, and *Type 3*. The reason for choosing these types of paper was motivated by their specific

properties, such as, (a) high dimensional stability regardless of temperature, (b) smooth surfaces, (c) free from contamination. In detail, mechanical parameters, electrical parameters (capacitance), and printability by inkjet printing were analyzed to select the most suitable paper for manufacturing humidity sensors. Moreover, the sensor performances were comprehensively studied.

2. Materials and Methods

2.1 Types of studied paper

In this work, the three types of commercial paper from Felix Schoeller Group denoted as *Type 1*, *Type 2*, and *Type 3* were studied. All three types have the same cross-sectional structure, consisting of raw paper in the middle, a resin coating bellow the raw paper, and a gloss coating (primer layer or nanoporous coating) on the top. *Type 1* has a total thickness of around 115 μm and grammage of 190 g/m^2, *Type 2* has a thickness of around 210 μm and grammage of 200 g/m^2, whereas *Type 3* has a total thickness of 175 μm and grammage of 170 g/m^2. These papers were designed for printing electronic components as substrates, which has a smooth surface and appropriate surface properties when silver inks are used for manufacturing components with high precision. The good interaction between the paper's coating and silver ink makes printing sensor on paper substrate reliable. Internal fibres structure of these papers provides high dimensional stability, which ensures less broke when constructing flexible printed sensors.

2.2 Characterization techniques

The following instruments were used for paper characterization. (1) For the analysis of morphological and topographic properties a JEOL JSM 6460 LV scanning microscope (SEM), with an EDS, was used. (2) For surface roughness analysis, Atomic Force Microscope (AFM), Veeco di CP-II as well as 3D Optical Profilometer, Huvitz microscope with Panasis software were used. (3) For mechanical characterization, a nanoindentation method was used, with a G200 nanoindenter, having a Berkovich diamond indenter with a face angle of 65.2°. (4) For humidity characterization, an Owlstone system was employed. This Owlstone system is an integrated test platform incorporating a humidity generator and a flow controller with exact measurement of temperature, flow, and humidity. The system can be used to produce a range of relative humidity concentrations from 40% up to 90% RH, with accuracy of ±1%. (5) Measuring contact angle and contact angle hysteresis was carried out by means of the sessile drop technique. Liquid droplet of about 2 μL volume was dropped on the surface of the analysed papers with a micropipette and image of the droplet was captured by a digital camera (Tucsen camera, Xintu Photonics) being attached to a microscope (Microzoom, Bausch and Lomb) with magnification of 2.25x and computed with the software IDS camera manager. The recorded droplet image was analysed with the help of the DropSnake method implemented as a Java plug-in for the ImageJ software and which is based on B-spline snakes (active contours) to shape the drop.[19]

3. Results and Discussion

3.1 Profilometer analysis

To discover the internal structure of the three types of studied paper, profilometer analysis was conducted. The optical profiler was used to record 2D and 3D surface profiles of each sample allowing the evaluation of the exact structure inside the papers, because it obtains a very large number of surface pictures from bottom to top and creates a single picture in two dimensions. The obtained 2D images are presented in Fig. 1, where *Type 1* is magnified 20 times, *Type 2* is magnified 50 times, and *Type 3* is magnified 20 times.

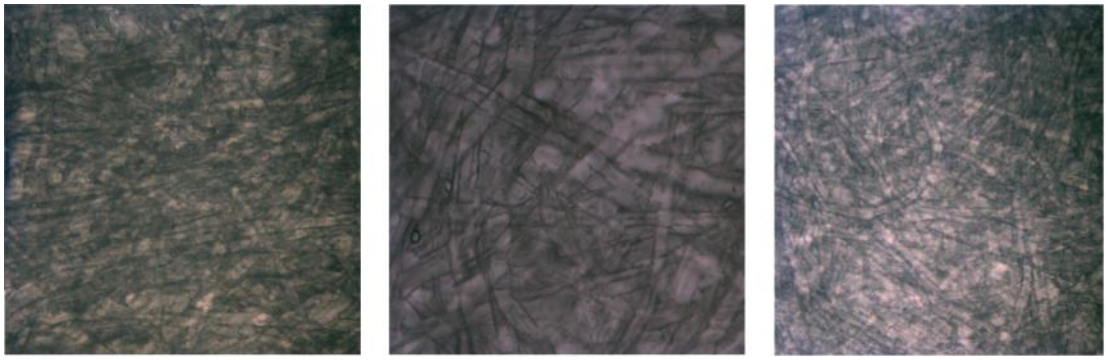

(a) (b) (c)

Fig. 1. (Color online) 2D profilometer images of studied papers: (a) *Type 1*, (b) *Type 2*, and (c) *Type 3*.

From Fig. 1, it can be seen that cellulose fibers are the main constituent of each paper. The paper fibers have a similar shape and size, and there is little difference in the internal structure of all three types of paper. The internal structure of the papers demonstrated that they are suitable for the fabrication of electronic structures by inkjet printing because the fibrous structure is capable of absorbing applied functional inks. The good interaction between the paper's coatings and different inks can create reliable organic and printed electronics components.

3.2 SEM results

Structural characterization was performed with an SEM to obtain exact cross-sectional views of the paper layers. SEM micrographs of the three types of studied paper with magnification of around 500 times are presented in Fig. 2.

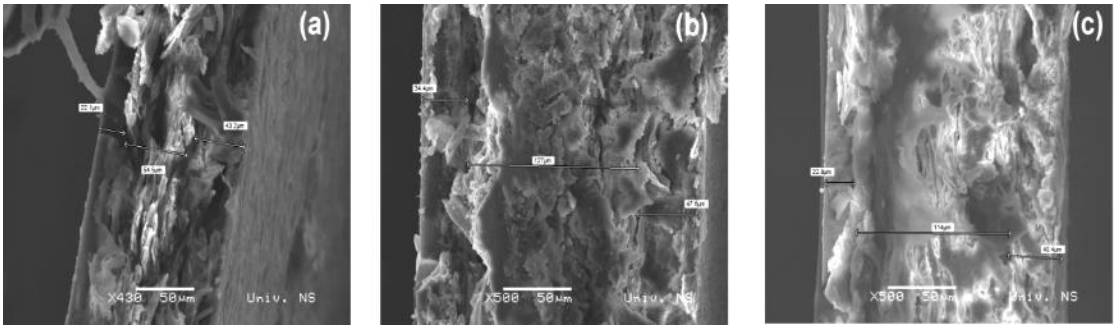

Fig. 2. (Color online) SEM micrographs of papers: (a) *Type 1*, (b) *Type 2*, and (c) *Type 3*.

From the SEM micrographs, the structure of the papers with the gloss layer, raw paper, and resin coating, looking from left to right, is clearly visible, including their thicknesses.

3.3 Surface characterization

To determine the surface roughness of the studied paper samples, AFM was used, since it is able to determine the surface topography of materials on the atomic scale vertically and on the nanometer scale horizontally. AFM images are presented in Fig. 3 for the three types of examined paper. Figures 3(a)-3(c) display the 3D surface and a 2D image of *Type 1*, *Type 2*, and *Type 3*, respectively.

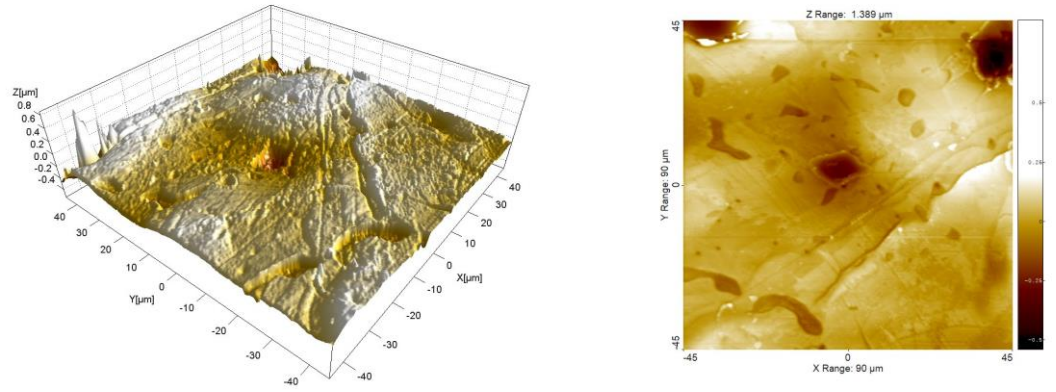

(a)

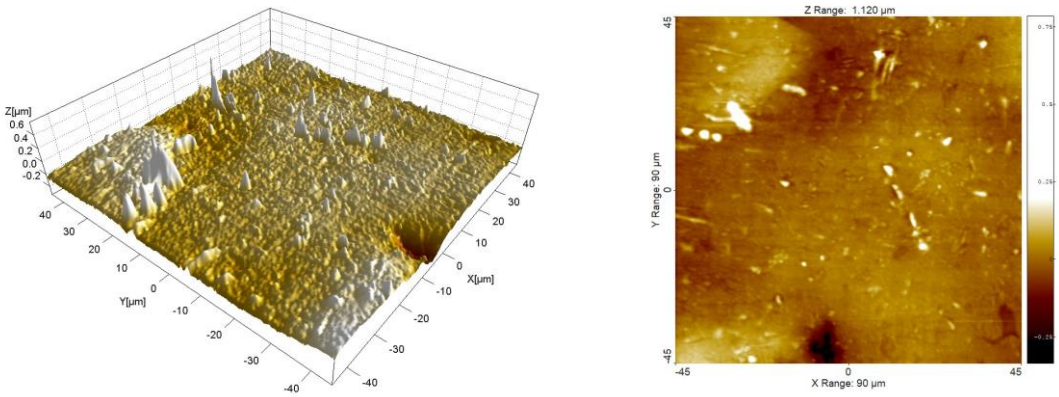

(b)

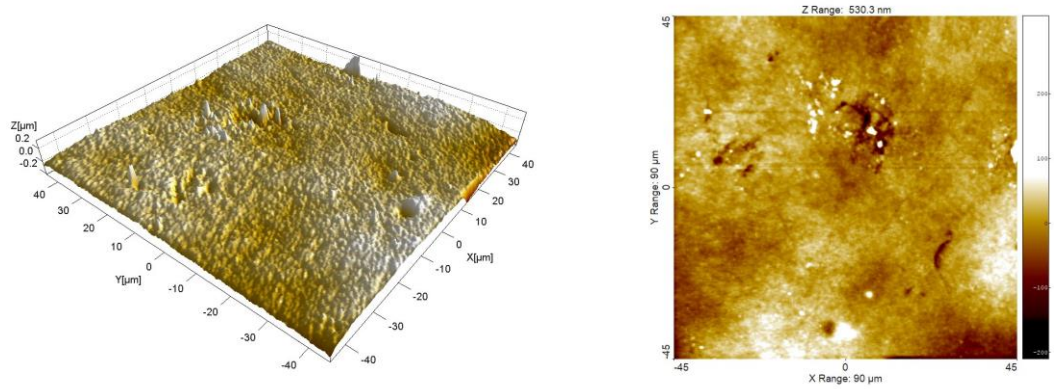

(c)

Fig. 3. (Color online) 3D and 2D AFM micrographs of papers: (a) *Type 1*, (b) *Type 2*, and (c) *Type 3*.

Surface roughness parameters for three papers are presented in Table 1. They were determined as average from four AFM images taken for each paper samples. Parameters Sci and Svi show how much fluid might be stored in core and valley zones. For a Gaussian height distribution, Sci approaches 1.56, while Svi approaches 0.11. Large values of these indices indicate large void volumes in core, i.e. valley zone. Since values of these indices for all three samples are close to the values specific for a Gaussian height distribution, it might be said that neither of samples has some special ability to retain a fluid. Sdr presents ratio of actual surface area and projected area. For a totally flat surface, the actual surface area and the projected area plane are the same and Sdr = 0 %. When a surface is flat, contact angle depends on surface free energy. However, when surface is rough, for hydrophilic surfaces observed contact angle would be lower than true contact angle. This is under assumption the whole surface area is wetted.

Table 1

Surface roughness parameters. Sa – average surface roughness, Sq – root mean square, Sci – core fluid retention index, Svi – valley fluid retention index, Sdr – Surface Area Ratio.

	Sa [nm]	Sq [nm]	Sci	Svi	Sdr [%]
Type 1	68 ± 22	102 ± 35	1.27 ± 0.14	0.12 ± 0.03	1.297 ± 1.36
Type 2	35 ± 6	50 ± 6	1.43 ± 0.14	0.12 ± 0.01	0.21 ± 0.02
Type 3	25 ± 3	34 ± 3	1.5 ± 0.09	0.12 ± 0.02	0.12 ± 0.02

From measured average surface roughness and Sdr parameter one might expect the highest wetting for *Type 1* paper. However, wetting does not have to be complete, air pockets might be formed in surface cavities which would reduce the wetting (increase the contact angle). The surface roughness of paper as a substrate has effects on the line edge printing quality (Fig. 11(b)). The inkjet printed conductive (Ag) line edge roughness decreases with decreasing in the surface roughness of the paper substrate.

3.4 Mechanical characterization of the studied papers

The nanoindentation technique was employed to investigate the mechanical properties of small volumes of paper samples. The recorded load and depth of penetration were used to form the load–displacement curves which can be used to derive the hardness of papers, because the paper can be exposed to various mechanical stresses or scratches during practical application. Nanoindentation measurements for different sets of samples were carried out using a G200 nanoindenter equipped with a Berkovich triangular pyramidal diamond tip. A preset depth (maximum of 5 μm) was applied to the pyramidal indenter in contact with the paper surface. The indentation cycle was considered as a load–unload cycle; first a load was applied, then it was ramped up to a peak load and then load was maintained for a fixed time before unloading. The time to ramp up the load was set to 15 s, while the peak loading time was set to 10 s. Multiple nanoindentation tests were carried out with at least eight indentations made, to ensure repeatability of measured results. Figure 4 shows the mean load–displacement curves measured on the *Type 1*, *Type 2*, and *Type 3* papers.

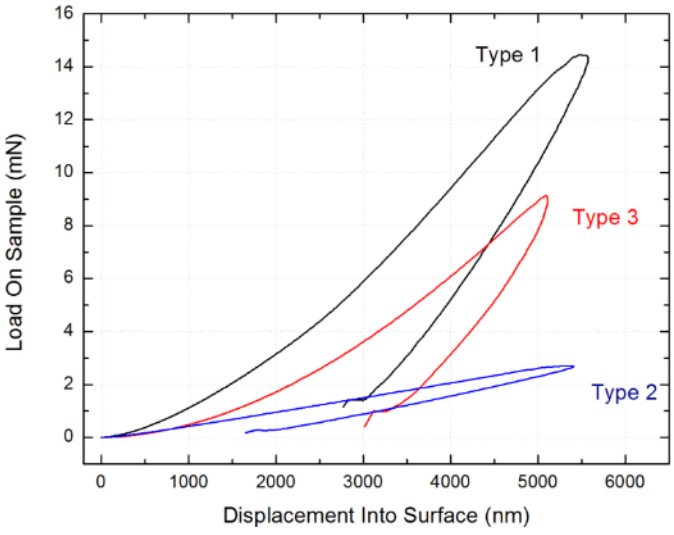

Fig. 4. (Color online) Load–displacement curves for analyzed papers.

Figure 4 shows that in the loading process, at maximum preset depth of 5 μm, the penetration load is around 15 mN for *Type 1*, 9 mN for *Type 3*, and 2 mN for *Type 2*. It can be noticed from Fig. 4 that the displacement into the surface exceeds the preset depth of 5 μm by approximately 500 nm. This happens when the Berkovich tip reaches the given preset depth and is held there for 5 s, as set in the initial conditions, the tip enters the material to a depth of a few more nanometers. It was confirmed that the raw paper layer was not reached (the thickness of gloss layer is 34 μm for *Type 2*, and around 22 μm for *Type 1* and *Type 3*, which can be seen from Fig. 2). The indentation curves for *Type 1* and *Type 2* show an increase in the indenter depth (secondary penetration) during the plateaus while the load is held, after loading and a decrease in the load at the end of the unloading curve. In almost all curves, viscoelastic return of the samples was

observed. It can be concluded from Fig. 4 that *Type 2* has the softest gloss layer because it needed the smallest load to reach the preset depth of 5 μm. Comparing the results of two other samples, both types have gloss coatings of similar thickness, but *Type 3* has a raw paper layer of almost twice the thickness of that of *Type 1*. Therefore, a smaller load is needed to reach the same preset penetration depth of 5 μm for *Type 3*. Figure 5 shows nanoindentation marks after evaluating the mechanical properties. They are in the shape of triangular pyramids on the paper substrate and the dimensions of the marks are also depicted in Fig. 5. The porous surface structure of the papers can be noticed from Fig. 5, which is advantageous for fabrication using inkjet printing.

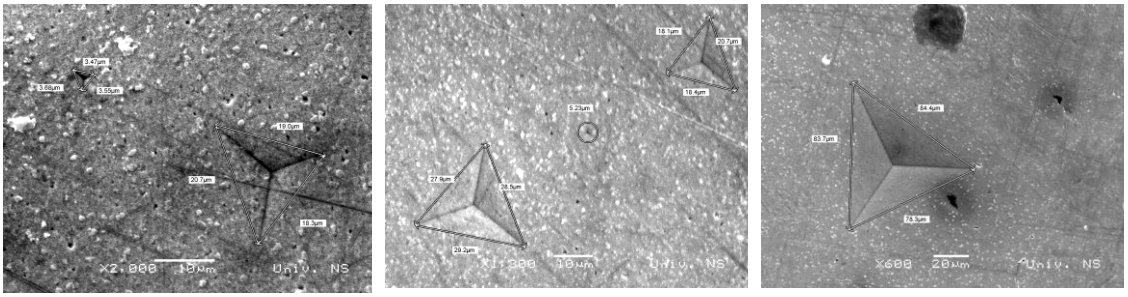

(a) (b) (c)

Fig. 5. (Color online) Marks after nanoindentation testing: (a) *Type 1*, (b) *Type 2*, and (c) *Type 3*.

3.5 Wettability of papers

Wetting properties are very important when inkjet printing process is applied. Because of that, we applied drop-shape analysis method for measuring static contact angles from optical images saved and analyzed with a software tool ImageJ (option drop_analysis). The variation of the static contact angle as a function of the time was measured (at room temperature and humidity around 60%) and results are presented in Fig. 6(a) for water droplet and Fig. 6(b) for silver ink droplets. Obtained contact angles for three types of studied paper were below 90°, which corresponds to high wettability. The paper *Type 2* had the highest contact angle, after that *Type 1* and *Type 3*. This proves the paper *Type 2* is the best as substrate in inkjet process due to its absorptive surface suitable for silver ink and can be applied for high temperatures. *Type 2* paper had a medium surface roughness, ensuring that the highest contact angle was measured. For papers *Type 1* and *Type 3* low contact angles indicate that wetting of the surface is favorable, and the ink will spread over a large area on the paper surface, which means that it is not so easy to obtain exact geometrical shape of the electronic components designed to be fabricated on the paper substrate. The obtained values for contact angle (Fig. 6) are slightly higher than reported contact angles in[20] for the same silver ink on polyimide (PI) film and silicon wafer substrates, where measured values were 10.6° and 16.3°, respectively. Furthermore, our results are comparable with the measured results presented in[21] for water (in the range from 8.079° to 36.412°) and for Ag nanoparticle ink (in the range from 8.293° to 19.949°) on different substrates (glass, silicon, PET, ITO, PVA). The inkjet printing line width can be higher if the contact angle of the droplet with the substrate is higher. Thus, it can be concluded that the printing line width is influenced by the contact angle rather than by the surface roughness of the substrate.

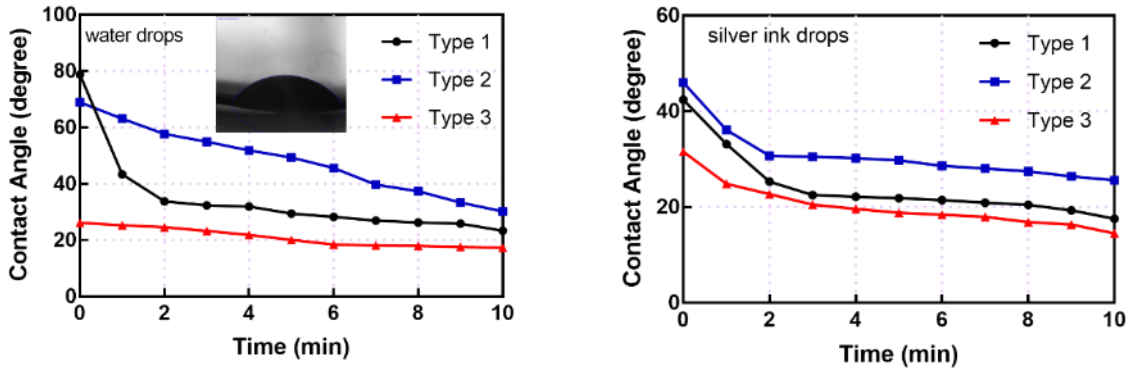

(a) (b)

Fig. 6. (Color online) Contact angle as a function of time (drop age) for (a) water drops, (b) silver ink drops, and for three types of analyzed paper.

The wettability is not just a static phenomenon. For paper surfaces, which are not homogeneous, there are domains or surface roughness, which prevents smooth drops motion. Because of that, we also measured a contact angle hysteresis, which are depicted in Fig. 7, for three types of examined papers. The behaviour is similar as for measured static angle.

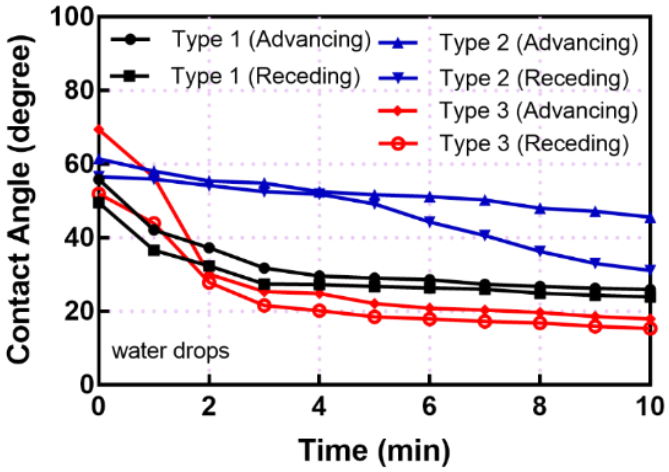

Fig. 7. (Color online) Contact angle hysteresis for three types of studied paper.

Furthermore, the surface tension of three types of paper was tested[18] and the measured values on the front side of the papers were: for *Type 1* = 55 ± 10 mN/m, for *Type 2* = 45 ± 10 mN/m, and for *Type 3* = 65 ± 10 mN/m. The strongest wetting was observed for *Type 3* paper, which is characterized by the highest surface tension, and the weakest wetting was observed for *Type 2* which demonstrated the lowest surface free energy. The results presented in Fig. 6 are in well agreement with these results for the surface tension. Higher the surface free energy means strongest the wetting and lower contact angle. High values of surface tension of paper substrates is an indication that conductive line will not be perfectly continual and silver ink might be uncontrollable spread over the surface during inkjet printing process.

3.6 Inkjet–printed dot array on different papers

Because of the intended application of the analyzed papers in printed and flexible electronics, dot arrays were printed on all three types of paper, to determine how each paper absorbs silver ink and which is the best as a substrate for flexible electronics. All dots were formed by inkjet printing, using a Dimatix DMP3000 deposition material printer.[22] Drops were printed on 2 mm × 2 mm pieces of paper, for all three analyzed samples to observe how each paper absorbs the applied functional ink. Before printing, the stand (holder) on which the paper was located was heated to 40 °C so that the silver ink did not spill out from the printing line on the gloss layer of the paper. Commercially available 50 wt% Sigma-Aldrich silver nanoparticle ink dispersed in tripropylene glycol monomethyl ether[23] was used to print dot array. Silver dots were printed then sintered at 100 °C for 30 min. Printed silver dots on the three types of studied paper are presented in Fig. 8. The distance between the centers of adjacent dots was 20 μm. The diameter of one drop of silver ink on the substrate was around 34 μm.

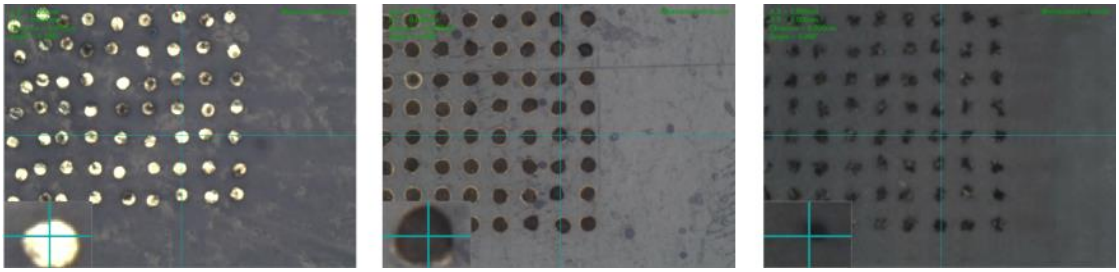

(a) (b) (c)

Fig. 8. (Color online) Dot arrays inkjet–printed on different papers: (a) *Type 1*, (b) *Type 2*, and (c) *Type 3*.

As shown in Fig. 8(a), the silver ink has a poor reaction with *Type 1* and the light color of the dots indicates that sintering has not been fully completed. This is the consequence of that fact that *Type 1* paper has no nanoporous coating on the top. From Fig. 8(c) it can be seen that the drops are not in designed circular shape, which is a consequence of highest surface tension of the *Type 3* paper. This is also a result of extremely smooth surface of this paper (Fig. 3(c)), which may produce drop spillage effect· *Type 2* has the best reaction with the silver ink and the drops are circular, as can be seen from Fig. 8(b). The thicknesses of the layers and their ratio (gloss layer to raw paper) affect the absorption capacity of the silver ink during the inkjet printing. For the Sigma-Aldrich silver nanoparticle ink used during the fabrication, the best choice is *Type 2*. The ink was seamlessly absorbed and uniform printing was achieved. The thinner gloss layer *for Type 1* causes that the ink to be mostly retained in the top gloss layer, which results in faster sintering during the heating of the holder, while the greater thickness of the raw paper relative to the gloss layer of *Type 3*, means that it absorbs too much ink, and well–formed dots are not produced during the printing. Thus, it can be concluded that the best paper for future application in the field of printed and flexible electronics is *Type 2*.

3.7 Humidity sensor on paper substrate

Paper is principally made of cellulose fibers, which possess hygroscopic properties. This induces variation of the electrical components in a circuit and degrades its metal deposits and the substrate itself. The experimental set-up and equipment for measurement are depicted in Fig. 9. Humidity generator was used for ensuring adequate humidity in the range from 40 to 90 % in the test chamber (a glass bottle), regulating input and output wet air flow. Fabricated sensor (Fig. 11) was placed into this test chamber and two wires were connected with two electrodes of interdigitated capacitor, from one side, and from another side these two wires were attached in the sample holder of the LCZ meter HP4277A. The measurement was carried out in laboratory conditions, and the temperature range was from 23.2 to 23.6 °C.

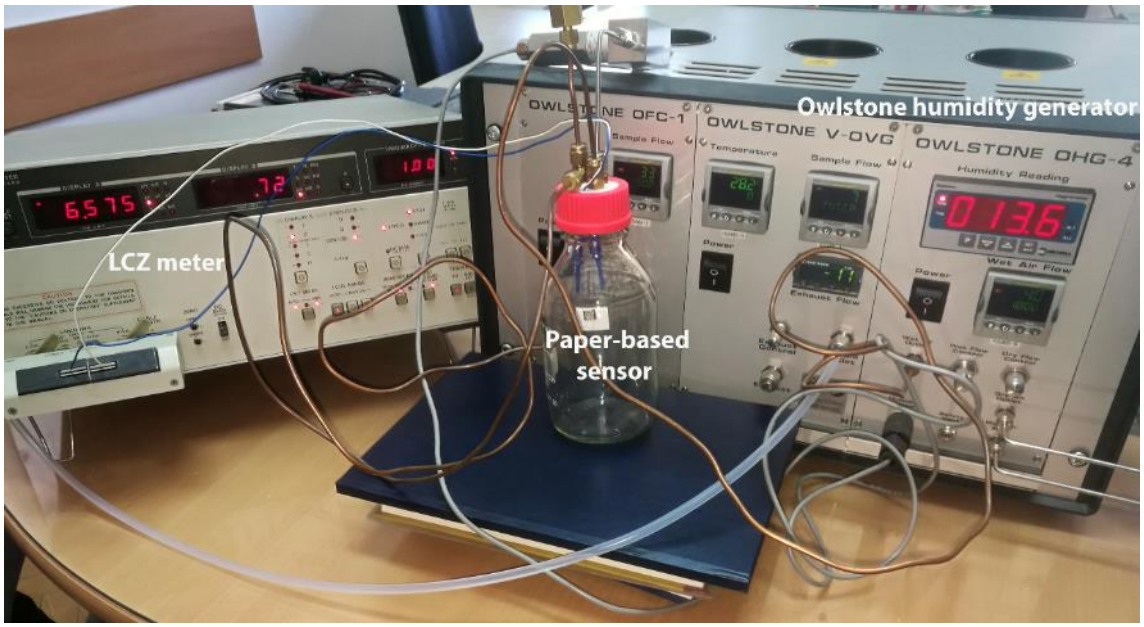

Fig. 9. (Color online) Experimental set-up for testing humidity sensor.

To measure the humidity, an interdigitated capacitive electrode structure was printed using inkjet printing, only on the *Type 2* paper, because it showed the best results after dot arrays printing with the silver nanoparticle ink, as demonstrated in the previous subsection. Figure 10 shows the design of the interdigitated electrode structure composed of nine electrodes with their corresponding dimensions. The overall dimension of the capacitor was 8.6 mm × 5.9 mm, the length of each electrode was 5 mm, while the width and the gap were 0.3 mm and 0.4 mm, respectively.

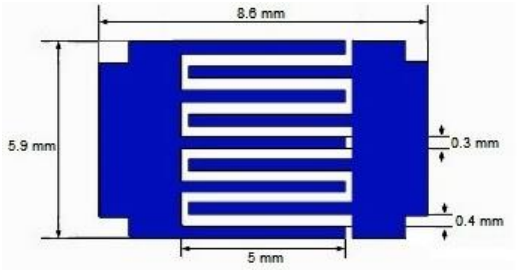

Fig. 10. (Color online) Designed interdigitated electrode structure with corresponding dimensions.

Figure 11(a) displays the printed interdigitated structure on the *Type 2* paper, whereas Fig. 11(b) presents a conductive line edge of the printed structure on this paper. It can be observed that the printing layer is uniform and that the edge is formed without spraying silver ink drops over surrounding area. The surface roughness of paper as a substrate has effects on the line edge printing quality (Fig. 11(b)). The inkjet printed conductive (Ag) line edge roughness decreases with decreasing in the surface roughness of the paper substrate.

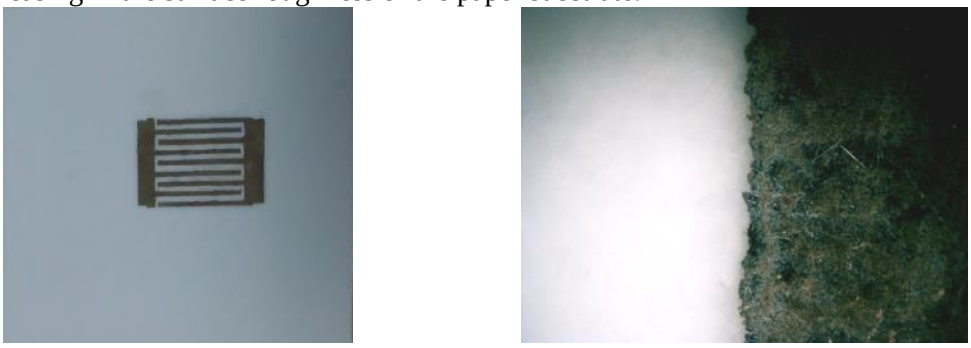

(a) (b)

Fig. 11. (Color online) Interdigitated electrode structure manufactured on *Type 2* paper, using inkjet method, (a) appearance after printing, (b) enlargement of a conductive line edge of the printed component.

In the case of an interdigitated capacitor, the electric field lines are closed also through the substrate, which is paper in our case, and the other part of electrical field are closed through the air which represents the dielectric between the fingers of the interdigitated capacitor. With increasing air humidity, the airflow is increased, which directly increases the capacitance of the interdigitated capacitor. With decreasing humidity, the permittivity decreases, which also reduces the capacitance of the interdigitated electrode structure.

Figure 12 depicts the variation of the sensor capacitance as a function of relative humidity in the range from 40 to 90%, with increasing and decreasing humidity. The interdigitated capacitive (IDC) paper-based sensor demonstrated slight hysteresis between the up and down cycles. The reason for this phenomenon is that surface of the paper reacts with moisture. When it exposed to different humidity levels, the printed sensor adsorbs and desorbs different amounts of water molecules from the surrounding ambient. If the relative humidity (RH) has higher values, the sensor will absorb more water vapor molecules. Afterwards, if RH is reduced to the initial low level of 40%, it will take more time to desorb and to reach equilibrium. Using paper as a substrate means that the adsorption process might be relatively fast, whereas the desorption process will be slower to achieve equilibrium due to the cellulose fibres in the internal structure of the paper.

These cycles showed an increase in RH (Up) and a decrease in relative humidity (Down) for the single measurement cycle at 100 kHz (shown in Fig. 12). The nonlinear fitting curves are also displayed. The water molecules would accumulate and inter-interacting cohesion forces would increase exponentially after reaching a threshold as evidence by water activity versus sorption isotherm. Changes in water profile affects the permittivity, and consequently causing the capacitance changed. The cohesion and adhesion of the water molecules depend on the structure of *Type 2* paper, which is presented by SEM and AFM micrographs. The hysteresis can be reduced by using a thinner paper, because it will take less time for the paper structure to dissolve water molecules and reach the equilibrium state.

The reproducibility of the inkjet–printed sensor was tested at 20 min intervals with RH increased and decreased in steps in the range from 40 to 90%. The time period of 20 min was set to allow the diffusing water molecules to be adsorbed between the electrodes (fingers) of the IDC structure and to stabilize RH. The reproducibility of the sensor, when exposed to different RH values over a period of about 4 h at room temperature, is shown in Fig. 13.

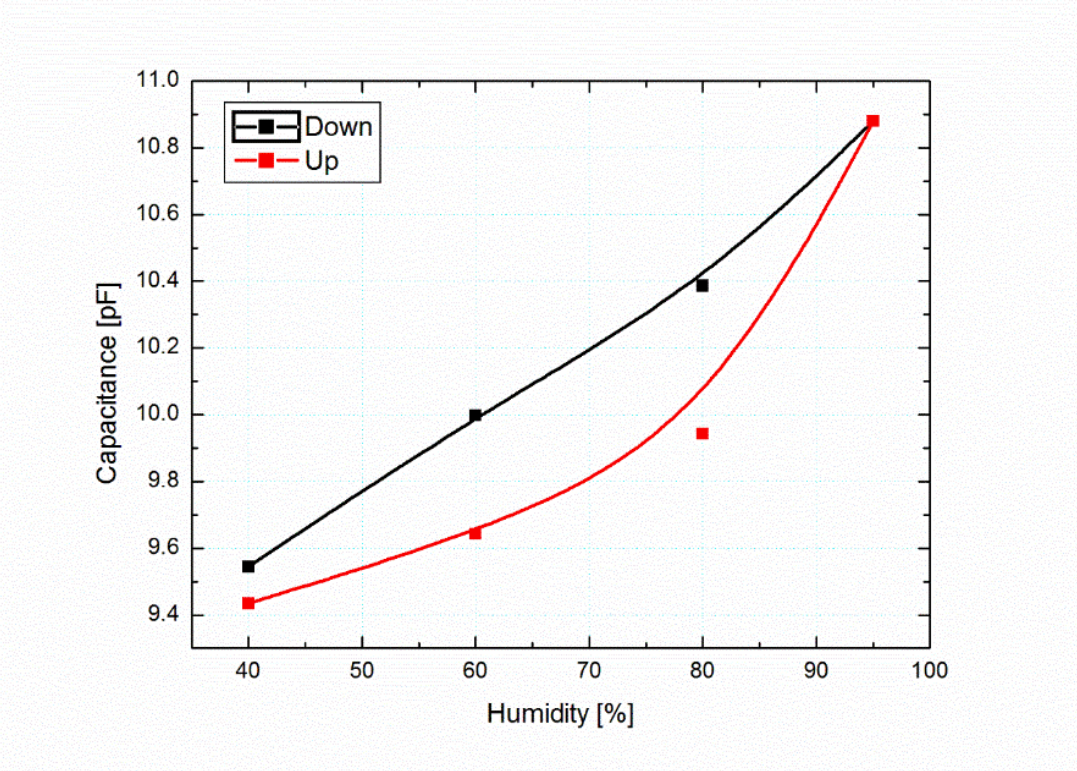

Fig. 12. (Color online) Behavior of inkjet–printed sensor in an Up–Down cycle in the interval of 40 – 90% RH. The Up (in red) and Down (in black) curves correspond to the adsorption and desorption processes, respectively.

The dynamic response of the printed sensor shows the repeatability of the results during a period in which RH changes over time. After 20 min of holding RH at 40% for which the capacitance of the printed sensor is 9.45 pF, about 5 min is required for sensor to respond to a higher RH. The printed sensor has a capacitance of about 10 pF at a higher RH of 60%. After that, RH is returned to 40%, for 20 min during which the sensor returns to the previous capacitance, than RH increased to 90%, at which the capacitance was about 10.6 pF.

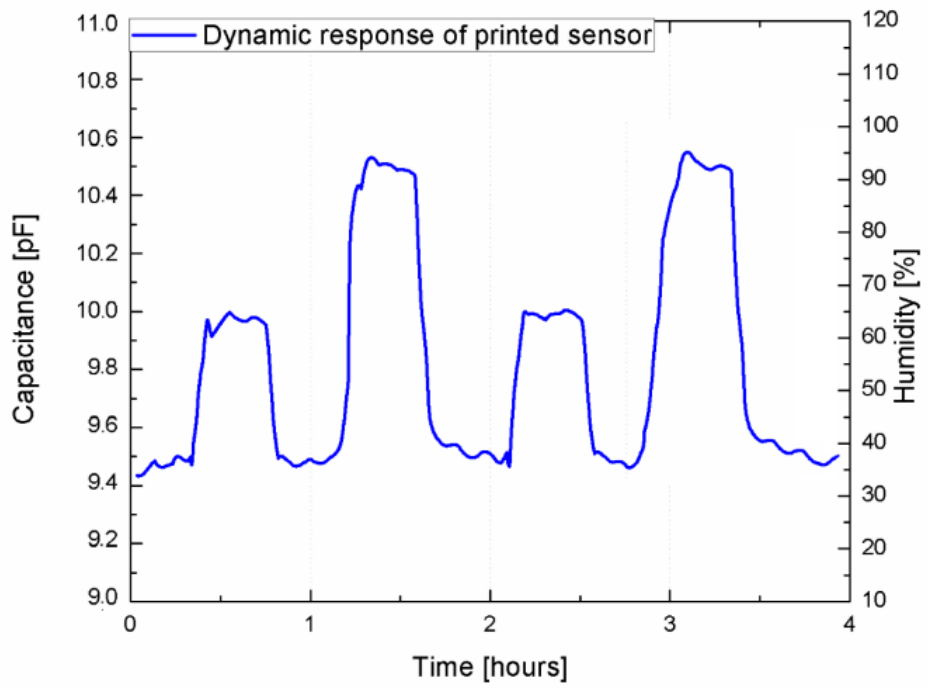

Fig. 13. (Color online) Dynamic response of a printed IDC sensor at a frequency of 100 kHz.

4. Conclusions

The use of papers in microelectronics and flexible electronics is currently in its infancy. In this work we comprehensively studied internal structures of fibers of three types of paper (using optical profilometer), their surface roughness characteristics (using AFM), cross-sectional structure (using SEM) and hardness (using nanoindenter). Among the analyzed papers as substrates, the most promising type of the paper for inkjet printed sensor is *Type 2*. This paper has precoating and after that nanaporous coating (both part of a gloss layer) at the top of its cross-section. This work proved that surface roughness should not be so high (*Type 1*), but also not extremely smooth (*Type 3*), and this compromise the paper *Type 2* satisfied. The *Type 2* has the lowest surface tension ensuring excellent quality of inkjet printed lines as well as the lowest mechanical hardness that is also a promising property for realization of the entire sensor system that can be flexible and to be applied to conform a desired shape. The incorporation of suitable papers in the process of inkjet printing is innovative, economical, and efficient, and has great potential for applications. The most suitable paper was selected for fabrication of humidity sensor and graphs of capacitance as a function of humidity and capacitance as a function of time were provided. The humidity–detection features of papers can play a significant role in the suitability and quality of the printing process and the final product. Accordingly, applications of papers for inexpensive sensors have great promise at the industrial scale, but comprehensive characterization and accurate profiling of the features of papers are required, as performed and described in this study.

Acknowledgments

Results presented in this article received funding from the EU Horizon 2020 research and innovation programme under the MSC Grant agreement no. 690876—MEDLEM, and being partly supported by the project 142-451-2459/2018-03. The authors would like to thank Schoeller Technocell GmbH & Co. KG for valuable comments. Authors are also grateful to colleagues (G. Dubourg) from the Biosens Institute, UNS for assistance in measuring contact angles.

References

1 C. Yang, H. Gu, W. Lin, M. M. Yuen, C. P. Wong, M. Xiong, and B. Gao: Adv. Mater. **23** (2011) 3052. doi: 10.1002/adma.201100530
2 C. Paragua, K. Frigui, S. Bila, D. Baillargeat: Proc. of the 45th European Microwave Conference, (2015). doi: 10.1109/EuMC.2015.7345900
3 Q. Cheng, Z. Song, T. Ma, B. B. Smith, R. Tang, H. Yu, H. Jiang, C. K. Chan: Nano Lett. **13** (2013) 4969. doi: 10.1021/nl4030374
4 Y. Wang, H. Guo, J. J. Chen, E. Sowade, Y. Wang, K. Liang, K. Marcus, R. R. Baumann, Z. Sh. Feng: ACS Appl. Mater. Interfaces **8** (2016) 26112. doi:10.1021/acsami.6b06704
5 A. C. Siegel, S. T. Phillips, M. D. Dickey, N. Lu, Z. Suo, G. M. Whitesides: Adv. Funct. Mater. **20** (2010) 28. doi: 10.1002/adfm.200901363
6 A. Määttänen, P. Ihalainen, P. Pulkkinen, S. Wang, H. Tenhu, J. Peltonen: ACS Appl. Mater. Interfaces **4** (2012) 955−964, dx.doi.org/10.1021/am201609w
7 O. S. Kwan, H. Kim, H. Ko, J. Lee, B. Lee, C. H. Jung, J. H. Choi, K. Shin: Carbon **58** (2013) 116. https://doi.org/10.1016/j.carbon.2013.02.039
8 M. Balde, F. Jacquemoud-Collet, A. V. B. Sorli: Sens. and Actuators A **240** (2016) 118. doi: https://doi.org/10.1016/j.sna.2015.09.037
9 M. Santhiago, C. C. Corrêa, J. S. Bernardes, M. P. Pereira, L. J. M. Oliveira, M. Strauss, C. C. B. Bufon: ACS Appl. Mater. Interfaces **9** (2017) 24365. doi:10.1021/acsami.7b06598
10 S. Cinti, M. Basso, D. Moscone, F. Arduini: Anal. Chim. Acta **960** (2017) 123. https://doi.org/10.1016/j.aca.2017.01.010
11 S. Cinti, C. Minotti, D. Moscone, G. Palleschi, F. Arduini: Biosens. Bioelectron. **93** (2017) 46. https://doi.org/10.1016/j.bios.2016.10.091
12 A. Russo, B. Y. Ahn, J. J. Adams, E. B. Duoss, J. T. Bernhard, J. A. Lewis: Adv. Mater. **23** (2011) 3426. https://doi.org/10.1002/adma.201101328
13 A. T. Singh, D. Lantigua, A. Meka, S. Taing, M. Pandher, G. Camci-Unal: Sensors **18** (2018) 2838. doi: 10.3390/s18092838
14 Z. Yu, Y. Tang, G. Cai, R. Ren, D. Tang: Anal. Chem. **91** (2019) 1222. doi: 10.1021/acs.analchem.8b04635
15 J. Sarfraz, P. Ihalainen, A. Maatanen, J. Peltonen: Thin Solid Films **534** (2013) 621. doi: https://doi.org/10.1016/j.tsf.2013.02.055
16 E. Linvill, P. Larsson, S. Ostlund: Mater. Des. **128** (2017) 231. doi:10.1016/j.matdes.2017.05.002
17 E. Linvill and S. Ostlund: Exp. Mech. **64** (2014) 1329. doi: 10.1007/s11340-014-9898-7
18 Special papers for printed electronics: https://www.felix-schoeller.com/en_en/business-unit/other-specialty-papers/p-esmartr.html (accessed July 2019)
19 A. F. Stalder, G. Kulik, D. Sage, L. Barbieri, P. Hoffmann: Colloids And Surfaces A: Physicochemical And Engineering Aspects, **286** (2006) 92.
20 M. Y. Chuang: Protocols and Reports. Paper **51** (2018) https://repository.upenn.edu/scn_protocols/51 (accessed August 2019)
21 V. K. S. Yadav, G. Natu, R. Paily: IEEE Transactions on Components, Packaging and Manufacturing Technology, **8** (2018) 1678. doi: 10.1109/tcpmt.2018.2854629
22 DMP-3000 Materials Printer: https://www.fujifilmusa.com/press/news/display_news?newsID=880182 (accessed July 2019)
23 Silver nanoparticle ink: https://www.sigmaaldrich.com/catalog/substance/silvernanoparticleink1078798765?lang=en&region=SX (accessed July 2019)